Coherent low-frequency motions of hydrogen bonded acetic acid dimers in the liquid phase

Karsten Heyne,[a] Nils Huse, Jens Dreyer, Erik T. J. Nibbering, and Thomas Elsaesser
Max-Born-Institut für Nichtlineare Optik und Kurzzeitspektroskopie, Max-Born-Strasse 2A, D-12489 Berlin, Germany

Shaul Mukamel
Department of Chemistry, University of California, Irvine, California 92697-2025

(Received 18 February 2004; accepted 22 April 2004)

Ultrafast vibrational dynamics of cyclic hydrogen bonded dimers and the underlying microscopic interactions are studied in temporally and spectrally resolved pump–probe experiments with 100 fs time resolution. Femtosecond excitation of the O–H and/or O–D stretching mode gives rise to pronounced changes of the O–H/O–D stretching absorption displaying both rate-like kinetic and oscillatory components. A lifetime of 200 fs is measured for the $v=1$ state of the O–H stretching oscillator. The strong oscillatory absorption changes are due to impulsively driven coherent wave packet motions along several low-frequency modes of the dimer between 50 and 170 cm^{-1}. Such wave packets generated via coherent excitation of the high-frequency O–H/O–D stretching oscillators represent a clear manifestation of the anharmonic coupling of low- and high-frequency modes. The underdamped low-frequency motions dephase on a time scale of 1–2 ps. Calculations of the vibrational potential energy surface based on density functional theory give the frequencies, anharmonic couplings, and microscopic elongations of the low-frequency modes, among them intermolecular hydrogen bond vibrations. Oscillations due to the excitonic coupling between the two O–H or O–D stretching oscillators are absent as is independently confirmed by experiments on mixed dimers with uncoupled O–H and O–D stretching oscillators. © *2004 American Institute of Physics.* [DOI: 10.1063/1.1762873]

I. INTRODUCTION

Multiple hydrogen bonds represent a key structural feature existing in a large variety of molecular systems. Hydrogen bonded liquids like water and alcohols form extended networks with different local geometries of the interacting molecules. The structure of biomolecules, the most prominent being double-stranded DNA, is determined by hydrogen bonds between the nucleic acid base pairs and, in a more general sense, protein structures are stabilized by hydrogen bonding interactions. There has been impressive progress in elucidating hydrogen bonded molecular structure over the last decades. In contrast, the dynamics of hydrogen bonds which occur on a multitude of time scales, and the underlying microscopic coupling and interaction mechanisms are much less understood.

Vibrational spectra provide information on local properties of hydrogen bonded groups, in particular the local geometry and overall interaction strength.[1] The stretching bands of the hydrogen donor groups, e.g., O–H or N–H groups, display a pronounced redshift of their center frequencies upon hydrogen bonding and substantial changes of their spectral envelopes. The line shape of the stretching bands reflects the microscopic interactions giving rise to hydrogen bond formation and governing the vibrational dynamics on a time scale between several tens of femtoseconds and several picoseconds. Though such phenomena have been studied extensively by steady-state vibrational spectroscopy and/or theoretical calculations, most vibrational spectra and, thus, the underlying interactions are not understood in detail. This lack of specific knowledge is caused mainly by the occurrence of different coupling mechanisms of similar strength leading to rather congested vibrational line shapes. In the condensed phase, both couplings related to hydrogen bonding and the interaction with the environment are important.

Time-resolved nonlinear vibrational spectroscopy allows us to separate the different coupling processes via their different microscopic dynamics occurring in the ultrafast time domain. Pump–probe as well as photon echo studies using broadband femtosecond mid-infrared pulses for inducing vibrational excitations have been reported for a variety of hydrogen bonded systems.[2,3] In water and related systems, the dephasing of coherent O–H stretching excitations, spectral diffusion processes within the broad O–H stretching band, vibrational relaxation, and energy transfer from excited molecules to the surroundings have been investigated[4–12] and, to some extent, modeled theoretically.[13–15] Underdamped nuclear motions which modulate the length of a hydrogen bond with a frequency on the order of 100 cm^{-1} have been observed after femtosecond excitation of O–H or O–D stretching oscillators in single intramolecular hydrogen bonds.[16–18]

Cyclic dimers of carboxylic acids represent particularly interesting model systems for studying intermolecular hydro-

[a]Author to whom correspondence should be addressed; Electronic mail: heyne@mbi-berlin.de

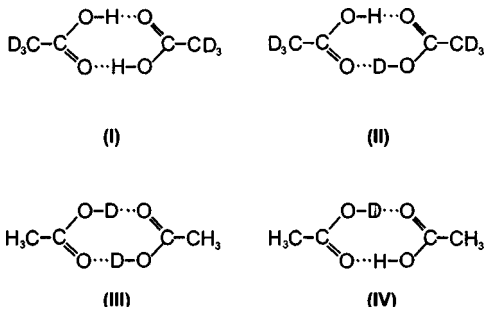

FIG. 1. Molecular structures of cyclic dimers: (I) pure methyl-deuterated acetic acid dimer, (II) mixed methyl-deuterated dimer containing one O–H and one O–D group, (III) pure carboxy-deuterated acetic acid, and (IV) mixed acetic acid dimer containing one O–H and one O–D group.

gen bonds in a well-defined geometry (Fig. 1). There exists extensive experimental and theoretical literature on the steady-state O–H and O–D stretching bands of such systems.[19–25] In addition, the coupling of the carbonyl oscillators has been investigated in femtosecond pump–probe and photon echo experiments[26] and transient spectra in the range of the O–H stretching band have been studied with picosecond time resolution.[27] Very recently, we reported femtosecond pump–probe studies providing the first evidence for coherent nuclear motions along several low-frequency modes of cyclic acetic acid dimers in nonpolar solutions.[28,29] Wave packet motion persists for several picoseconds, whereas coherent polarizations on O–H stretching transitions display fast femtosecond dephasing.[30]

In this paper, we present an in-depth study of low-frequency vibrational coherences in cyclic dimers of acetic acid, combining femtosecond pump–probe spectroscopy in the mid-infrared and *ab initio* calculations based on density functional theory. Pump–probe experiments on cyclic dimers of acetic acid, deuterated acetic acid, and mixed dimers with one O–H and one O–D group allow for separating anharmonic couplings between high- and low-frequency modes from other types of interactions, in particular from excitonic coupling between two resonant O–H/O–D stretching oscillators. Femtosecond excitation of the stretching mode gives rise to oscillatory motions along several low-frequency modes enabling a clear separation between Fermi resonance coupling and coupling to low-frequency modes.

The paper is organized as follows: In Sec. II, we discuss the line shape of the steady-state O–H and O–D stretching bands focusing on the different microscopic couplings. The low-frequency vibrational spectrum of cyclic dimers is analyzed in Sec. III both from the theoretical and experimental point of view. Our pump–probe studies are presented in Sec. IV, followed by a discussion of experimental and theoretical results in Sec. V. Conclusions are presented in Sec. VI.

II. LINE SHAPE OF O–H AND O–D STRETCHING BANDS IN HYDROGEN BONDED DIMERS

The line shape of the O–H and/or O–D stretching band of acetic acid dimers has been studied both in the gas and the liquid phase.[19,22,23,25,31–34] In Figs. 2(a) and 2(b), the O–H and O–D stretching absorption is shown for acetic acid and

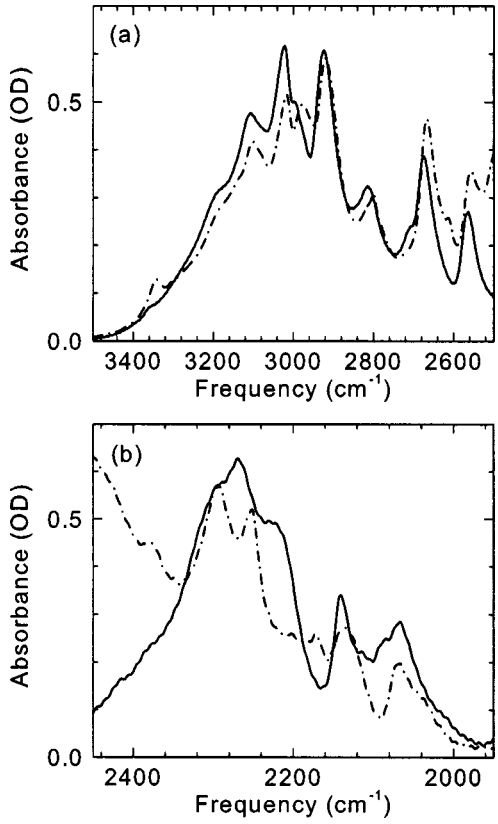

FIG. 2. (a) Solid line: O–H stretching band of cyclic acetic acid dimer (I) dissolved in CCl_4. Dot-dashed line: O–H stretching band of mixed cyclic acetic acid dimer (II). (b) Solid line: O–D stretching band of cyclic acetic acid dimer (III) dissolved in CCl_4. Dot-dashed line: O–D stretching band of mixed cyclic acetic acid dimer (IV). At high frequencies the low energy part of the O–H stretch absorbance also contributes.

deuterated acetic acid dissolved in CCl_4, respectively (concentration $c \simeq 0.8\,\mathrm{M}$). The cyclic dimers represent the predominant species under such conditions.[21] Upon hydrogen bonding, both stretching bands display a strong redshift due to a reduced force constant compared to free O–H or O–D groups, a pronounced broadening, and a substructure with several local absorption maxima.

Such complex line shapes have been analyzed in theoretical studies taking into account the following microscopic couplings:[19,22,23,25,31–34]

(i) Anharmonic coupling to low-frequency modes. Upon formation of hydrogen bonds, the O–H/O–D stretching oscillator becomes increasingly anharmonic, resulting in an enhanced coupling between high-frequency stretching and low-frequency modes of the hydrogen bonds. As the time scales of nuclear motions along the low- and high-frequency degrees of freedom differ by a factor on the order of 20, anharmonic coupling has been described in terms of a Born–Oppenheimer-like picture where the different states of the O–H or O–D stretching oscillator define a potential energy surface for the low-frequency modes (cf. Fig. 3). Dipole-allowed transitions from different levels of the low-frequency oscillator in the $v_{\mathrm{OH/OD}}=0$ state to different low-frequency levels in the $v_{\mathrm{OH/OD}}=1$ state lead to a progression of lines which is centered at the pure O–H/O–D stretching transition and displays a mutual line separation by one quan-

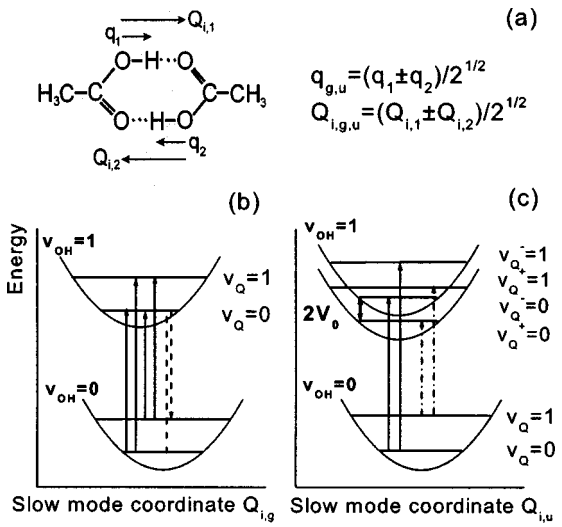

FIG. 3. (a) Schematic of the cyclic acetic acid dimer including high- ($q_{1,2}$) and low-frequency ($Q_{i,1,2}$) local mode coordinates. (b), (c) Schematic potential energy diagrams of low-frequency modes anharmonically coupled to the O–H stretching motion. The potential energy surfaces in the $v_{OH}=0$ and $v_{OH}=1$ states and the two lowest vibrational levels of the low-frequency mode are plotted as a function of the symmetrized low-frequency coordinates (b) $Q_{i,g}$ and (c) $Q_{i,u}$. For $Q_{i,u}$, the Davydov splitting $2V_0$ in the $v_{OH}=1$ state results in two series of vibrational transition lines (solid and dot-dashed arrows) from the $v_Q=0$ and $v_Q=1$ levels. Dashed line in (b): resonantly enhanced Raman process.

tum of the low-frequency mode. With increasing separation of the lines from the center, the absorption strength decreases because of decreasing Franck–Condon factors between the low-frequency levels involved. For each low-frequency mode coupling to an O–H/O–D stretching oscillator, an independent progression of lines occurs. In principle, this mechanism results in a strong broadening and/or spectral substructure of the overall O–H/O–D stretching band, even for a small number of absorption lines with large Franck–Condon factors.

(ii) Excitonic or Davydov coupling. In multiple hydrogen bonds, dipole–dipole and/or through–bond interactions can result in a coupling of local oscillators at the same transition energy. In the approach developed in Ref. 19 for the two O–H/O–D stretching oscillators, the $v_{OH/OD}=0$ states of the two O–H/O–D oscillators in cyclic carboxylic acid dimers are considered to be degenerate and coupling comes into play whenever one of the oscillators is excited. The excitonic coupling V_0 leads to a splitting of the $v_{OH/OD}=1$ states by $2V_0$.

The coupled system has been described by taking into account the C_{2h} inversion symmetry of the planar cyclic dimer and introducing symmetrized vibrational coordinates $q_{g,u}=(1/\sqrt{2})(q_1\pm q_2)$ and $Q_{i,g,u}=(1/\sqrt{2})(Q_{i,1}\pm Q_{i,2})$ for the stretching and the low-frequency modes Q_i, respectively. Considering both anharmonic and excitonic coupling and taking into account the dipole selection rules, the resulting line shape consists of two different progressions between the $v_{Qu}=0$ level of the $Q_{i,u}$ mode in the $v_{OH/OD}=0$ state and the $v_{i,Qu}^-$ levels in the $v_{OH/OD}=1$ state as well as between the $v_{Qu}=1$ level in the $v_{OH/OD}=0$ state and the $v_{i,Qu}^+$ levels in the $v_{OH/OD}=1$ state [Fig. 3(b)]. Simultaneously, the number of quanta in the $Q_{i,g}$ mode can be changed when exciting the system to the $v_{i,Q}^-$ or $v_{i,Q}^+$ levels, introducing an additional degeneracy of the lines in the respective progression. It is important to note that an individual molecule displays only one of those progressions, depending on whether the $v_{i,Qu}=0,2,4...$ or $v_{i,Qu}=1,3,5,...$ level is populated. In an ensemble of molecules at sufficiently high vibrational temperatures, several levels are populated and, consequently, both series of lines contribute to the overall vibrational band.

A comment should be made on excitations of the low-frequency modes in the ground state of the O–H/O–D stretching oscillators. Such excitations can be created by resonantly enhanced Raman scattering of infrared pulses overlapping spectrally with the O–H/O–D stretching band. In such a process, a first interaction with the electric field of the pulse promotes the system to the $v_{OH/OD}=1$ state from which it is projected down onto the final vibrational state by a second interaction [Fig. 3(b)]. For mixed dimers (II) and (IV) both interactions are resonantly enhanced by the dipole moment of the O–H/O–D stretching mode and both the $Q_{i,g}$ and $Q_{i,u}$ modes can be excited. For symmetric dimers (I) and (III), however, the dipole selection rules show that this resonance Raman process occurs between any state of the $Q_{i,g}$ mode, whereas for the $Q_{i,u}$ mode transitions between states with even and odd quantum numbers (e.g., v_{Qu} $0\rightarrow1$) are not allowed.

(iii) Fermi resonances between the $v_{OH/OD}=1$ states of the stretching mode and overtones or combination bands. Anharmonic coupling between the $v_{OH/OD}=1$ state of the O–H/O–D stretching oscillator and nearly isoenergetic overtone or combination vibrational states can lead to an additional splitting of the O–H/O–D stretching transition into different components with a relative shift determined by twice the respective coupling.[20] In addition to their pronounced influence on the line shape, Fermi resonances are considered to play a key role for intramolecular vibrational relaxation of the $v_{OH/OD}=1$ state.[13,35]

The first analysis of the O–H/O–D stretching band of cyclic acetic acid dimers in the gas phase has invoked anharmonic coupling to low-frequency modes and Davydov coupling.[19] Using a single low-frequency mode and empirical parameters for anharmonic and excitonic couplings, the main features of the experimental spectra were reproduced. This picture has been revised substantially in a later analysis in which Fermi resonances were included as well.[20] Now, the spectral substructure of the O–H stretching band was attributed to a number of Fermi resonances. This conclusion is supported by recent *ab initio* calculations on cyclic dimers of formic, acetic, and benzoic acid in the gas phase, giving a much stronger coupling of combination and/or overtones to the O–H stretching oscillator than of low-frequency hydrogen bond modes.[24] Even for dimers in the gas phase, however, a quantitative theoretical modeling of the O–H/O–D stretching band taking into account all such coupling and broadening mechanisms has not been done.

In the condensed phase, the O–H/O–D stretching band is additionally broadened by interaction of the cyclic dimers with the solvent. Overdamped intramolecular or solvent modes exert a fluctuating force on the O–H/O–D oscillators.

TABLE I. Harmonic frequencies ω_j, depolarization ratios ρ_j, and cubic force constants Φ_{i^2j} for $i=\nu_{OH/OD}(b_u)$ and low-frequency modes j (in cm^{-1}).

Low-frequency mode j	$(CH_3-COOH)_2$			$(CD_3-COOH)_2$			$(CH_3-COOD)_2$			$(CD_3-COOD)_2$		
	ω_j	ρ_j	ϕ_{i^2j}	ω_j	ρ_j	ϕ_{i^2j}	ω_j	ρ_j	ϕ_{i^2j}	ω_j	ρ_j	ϕ_{i^2j}
τ_{bg} methyl torsion	44	0.75	2[a]	33	0.75	−2[a]	44	0.75	2[a]	33	0.75	−3[a]
γ_{bg} dimer out of plane wagging	118	0.75	0	111	0.75	0	118	0.75	0	111	0.75	0
δ_{ag} dimer in-plane bending	159	0.65	151	155	0.67	148	156	0.67	111	153	0.67	109
ν_{ag} dimer stretching	174	0.07	−145	169	0.08	−143	174	0.09	−103	168	0.09	−102

[a]Φ_{ij^2}.

Depending on the modulation strength and time scale, the spectra may vary between a distribution of transition frequencies (inhomogeneous broadening) or a single motionally narrowed transition (homogeneous broadening). Very recently, we have presented the first femtosecond photon echo study of coherent O–H stretching polarizations in acetic acid dimers.[30] Anharmonic coupling of the O–H stretching mode and low-frequency modes results in a multilevel character of the vibrational coherence. Spectral diffusion within the O–H stretching band is negligible, i.e., the band displays a predominant homogeneous broadening. A vibrational dephasing time of approximately 200 fs was derived from the data.

III. LOW-FREQUENCY MODES OF CYCLIC DIMERS: THEORY AND VIBRATIONAL SPECTRA

Low-frequency vibrational modes for the isotopomers (I)–(IV) were analyzed by calculating harmonic normal mode infrared and Raman spectra as well as anharmonic couplings between high- and low-frequency normal modes. Geometry optimization and normal mode calculations were performed using density functional theory (DFT) with the B3LYP[36–39] functional and the 6-311+G(d,p)[40–42] basis set as implemented in GAUSSIAN 98.[43] Anharmonic coupling was introduced by expanding the potential energy V in a Taylor series up to fourth order in a selected set of N dimensionless normal coordinates q around the equilibrium geometry

$$V=\frac{1}{2}\sum_{i}^{N}\omega_i q_i^2+\frac{1}{6}\sum_{i,j,k}^{N}\Phi_{ijk}q_i q_j q_k + \frac{1}{24}\sum_{i,j,k,l}^{N}\Phi_{ijkl}q_i q_j q_k q_l, \quad (1)$$

where ω_i are the harmonic frequencies and the cubic and quartic force constants are given by

$$\Phi_{ijk\ldots}=\frac{\partial^n V}{\partial q_i \partial q_j \partial q_k \ldots}. \quad (2)$$

Cubic and semidiagonal quartic ($k=l$) force constants were generated numerically from analytical second order derivatives applying a finite difference procedure outlined by Schneider and Thiel.[44] Three-point finite difference formulas with a dimensionless displacement of 0.04 were used. To ensure sufficient numerical accuracy in the DFT calculation the default numerical integration grid was enlarged (grid =ultrafine, that is 99 radial shells with 590 angular points per shell).[45] Larger grids provided no additional improvement in accuracy.

Our study is restricted to the cyclic dimer geometry with C_{2h} symmetry, because other geometries such as the side-on or linear dimers are supposed to account only for a very small contribution of structures in the gas phase or in nonpolar solution, respectively.[46,47] The optimized geometry of the cyclic dimer is very similar to the one published previously by Emmeluth *et al.*[25]

Results of harmonic frequency calculations reveal the existence of eight low-frequency modes below 200 cm^{-1}. Subsequent modes follow above ≈400 cm^{-1}. Six of the low-frequency modes constitute intermolecular vibrations newly formed upon dimerization of the two acetic acid monomers. The other two are methyl torsion modes. Within the C_{2h} point group, four of the low-frequency modes are IR active (ungerade), whereas the other four are Raman active (gerade). For the calculation of anharmonic couplings we consider the four Raman active modes coupled to the IR active (b_u) high-frequency OH stretching mode (i). Harmonic frequencies for the low-frequency modes (ω_j), depolarization ratios ρ_j, and cubic coupling constants Φ_{i^2j} (Φ_{ij^2} for the methyl torsion mode) are compiled in Table I for all four isotopomers with identical monomers. These cubic coupling constants constitute the main contribution to the off-diagonal anharmonic couplings in the vibrational Hamiltonian[48] and thus will be used in the following to discuss the mode-specific strength of anharmonic coupling between high- and low-frequency modes.

Calculated low-frequency Raman spectra are plotted in Fig. 4 together with the cubic force constants Φ showing the strength of anharmonic coupling of the respective low-frequency modes to the $\nu_{OH/OD}$ mode. The character of the modes can be deduced from Fig. 5, where the arrows denote the relative amplitude of the normal coordinate elongations.

The methyl torsion mode (b_g) is calculated as lowest-frequency Raman mode, but with the largest Raman intensity among the low-frequency modes. Methyl deuteration leads to an isotopic shift of −11 cm^{-1}. It can be seen from Fig. 5 that the pure methyl torsion is not entirely decoupled from the carboxy group. The dimer out-of-plane (oop) wagging mode (b_g) follows at intermediate frequencies and intensities with an isotopic shift of −7 cm^{-1} upon methyl deuteration. Two totally symmetric modes are calculated at about 160 and 170 cm^{-1}, respectively, and assigned to the dimer in-plane (ip) bending and dimer stretching modes. They show isotopic redshifts in the order of 3–6 cm^{-1} both upon methyl as well as carboxy deuteration. Both of them exhibit strong variations of the intermonomer distance and thus of the hydrogen bonds. For all isotopomers, the methyl torsion

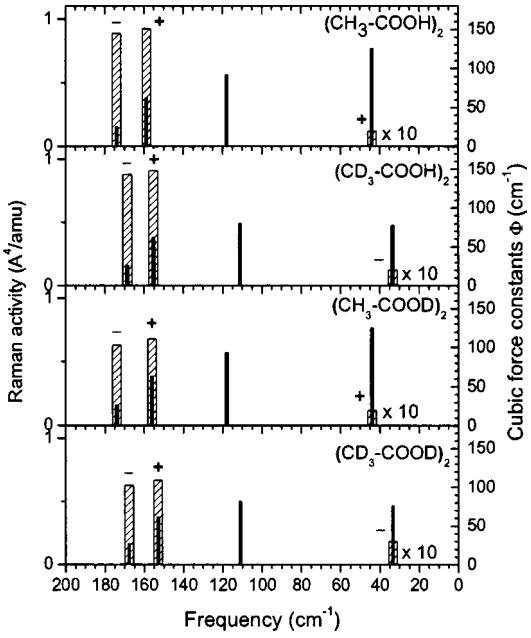

FIG. 4. Calculated normal mode low-frequency Raman spectra (solid bars, left ordinate) and cubic force constants Φ (open dashed bars, right ordinate). Plus and minus denote the sign of the force constants.

and dimer oop wagging modes are depolarized, the ip bending mode is slightly polarized, and the dimer stretching mode is strongly polarized. The ip bending and dimer stretching modes exhibit large anharmonic couplings to the O–H/O–D stretching mode with opposite sign. For all four isotopomers, the absolute coupling strength is somewhat larger for the bending than for the stretching mode. Anharmonic coupling to the methyl torsion mode is substantially smaller. The oop wagging mode is uncoupled. Whereas the influence of methyl deuteration on the anharmonic coupling is very small, carboxy deuteration decreases the coupling strengths by a factor of about 2/3.

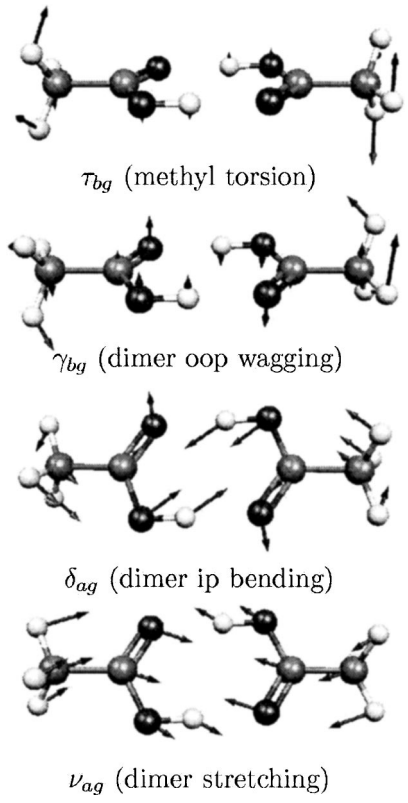

FIG. 5. Raman active low-frequency normal modes.

We now compare our results to previous work on low-frequency modes. Nielsen and Lund studied low-frequency Raman spectra of pure liquid CH_3COOH, CH_3COOD, and CD_3COOD at room temperature.[49] After subtraction of the elastic scattering contribution (Rayleigh wing), the very broad spectra were decomposed into three bands with maxima at ≈165, ≈115, and ≈55 cm^{-1}. The highest frequency band was found to be partially polarized, whereas the other two have depolarization ratios close to 0.75. Based upon the depolarization ratios and isotopic shifts they assigned the three bands to the three intermolecular vibrations of the cyclic dimers, that is the band at 55 cm^{-1} to the δ_{ag} ip bending mode, the 115 cm^{-1} band to the γ_{bg} oop wagging mode, and the band at 165 cm^{-1} to the ν_{ag} dimer stretching mode. The assignment of the 55 cm^{-1} band is not consistent with our present results.

Hartree–Fock (HF/6-31G(d,p)) calculations were performed for different dimer structures as well as a trimer, tetramer, and pentamer to analyze low-frequency Raman spectra of liquid acetic acid.[50] The experimental spectrum shows broad bands at 50, 120, and 170 cm^{-1}. Curve fitting analysis, however, reveals four peaks at 49, 118, 165, and 185 cm^{-1}. The HF calculation results in two strong bands at 84 and 119 cm^{-1}, assigned to methyl torsion and oop wagging motions, as well as two weak bands at 154 and 160 cm^{-1}, corresponding to the dimer stretching and bending modes. The assignment of the ip bending mode to the lowest-frequency band in Ref. 49 has been called into question.

A monomers-in-dimers model in up to six dimensions comprising stretching and bending modes of the carboxy group was developed to model the O–H/O–D stretching infrared spectra.[25] It is concluded that the coarse structure of high-resolution gas-phase infrared spectra measured with a ragout jet can be explained by anharmonic couplings solely within the carboxy groups of the monomers. It is suggested that Franck–Condon-type progressions of intermolecular low-frequency modes may account for the fine structure which is, however, not included in the Fermi resonance model used in this work.

Infrared spectra for the related formic and benzoic acid dimers were calculated from cubic anharmonic force fields including coordinates that couple the high-frequency O–H stretching mode to the O–H bending and to the intermolecular dimer stretching mode in the case of benzoic acid dimers and a full cubic force field in the case of formic acid dimers.[24] The calculations give cubic force constants for Fermi resonance coupling of ν_{OH} with the O–H bending mode that are about twice as large as force constants for coupling with the dimer stretch mode. The authors note, however, that their restricted cubic force field significantly underestimates the coupling to the low-frequency modes. It is concluded that the O–H bending Fermi resonance dictates

the width and much of the substructure of the ν_{OH} band, whereas coupling to low-frequency modes is unimportant, although it may contribute to the congestion of the spectrum.

In conclusion, none of the existing calculations has included all relevant coupling mechanisms. Thus, a quantitative understanding of the linear O–H/O–D stretching bands has not been reached. The calculations of Refs. 24 and 25 suggest that the coarse structure of the bands is dictated by Fermi resonances, whereas anharmonic couplings to low-frequency modes are much less apparent. As a result, it has not been possible to identify the relevant low-frequency modes and their anharmonic couplings by linear spectroscopy.

IV. ULTRAFAST PUMP–PROBE STUDIES OF VIBRATIONAL DYNAMICS

A. Experimental techniques

In our experiments, we studied solutions of acetic acid and deuterated acetic acid in the nonpolar solvent CCl_4. The concentrations were in a range between 0.2 and 0.8 M in which the cyclic dimer represents the predominant species in the sample.[21] Mixed dimers with one O–H and one O–D oscillator were prepared in CCl_4 by dissolving acetic and deuterated acetic acid with relative concentrations of 6:1 and 1:6 to study O–D and O–H stretching excitations, respectively. In the femtosecond experiments, samples with an optical thickness $A=-\log(T_0)\leqslant 0.6$ were studied at a temperature of 300 K (sample thickness 0.1 mm).

Ultrashort and widely tunable mid-infrared pulses of less than 100 fs were generated at a repetition rate of 1 kHz by parametric frequency conversion of regeneratively amplified pulses from a mode-locked Ti:sapphire laser.[51] Two-color pump–probe measurements were performed by exciting approximately 1% of the acetic acid dimers with a pump pulse of 1 μJ energy. An independently tunable weak probe pulse detects the resulting changes of vibrational absorbance as a function of pump–probe delay. After interaction with the sample, the probe pulse is dispersed and detected with a spectral resolution of about 6 cm^{-1} by a HgCdTe detector array. The absorbance change corrected for rotational relaxation $\Delta A_{iso}=(\Delta A_{\parallel}+2\Delta A_{\perp})/3$ was derived from measurements with parallel and perpendicular linear polarization of pump and probe pulses ($\Delta A_{\parallel}=-\log[T_{\parallel}(t_D)/T_{\parallel 0}]$; $T_{\parallel}(t_D)$, $T_{\parallel 0}$ sample transmission with and without excitation; t_D delay time).

B. Experimental results

1. Transient spectra

We performed ultrafast pump–probe measurements exciting the O–H/O–D stretching vibration at different frequencies and probing the complete spectral range of the O–H/O–D stretching band. The transient spectra taken at 0.5 ps [Figs. 6(a) and 6(b), solid lines] show predominantly a decrease of absorption[27] (bleaching and stimulated emission, negative sign) between 2600 and 3100 cm^{-1} and between 2050 and 2250 cm^{-1} for O–H and O–D excitation, respectively. Enhanced absorption is found on the low- and high-energy tails of the steady-state band [Figs. 2(a) and 2(b), solid lines]. The enhanced absorption on the low-energy tail of the spectrum is due to excited state absorption ($v_{OH/OD}=1\rightarrow 2$ transition, positive sign) which is redshifted with respect to the $v_{OH/OD}=0\rightarrow 1$ transition as a consequence of anharmonicity. It decays within several hundred femtoseconds. The $v_{OH/OD}=1$ state does not decay directly back to the thermally equilibrated $v_{OH/OD}=0$ state upon population (T_1) relaxation. Instead, a hot ground state $v_{OH/OD}=0'$ is reached in which the O–H/O–D stretching oscillator is deexcited, but other modes of the hydrogen bonded system, e.g., low-frequency hydrogen bond vibrations, contain vibrational excess energy. Anharmonic coupling with these excited modes results in a weakening of the hydrogen bond. Therefore, the $v_{OH/OD}=0'$ state absorbs on the high-energy side of the steady-state band and decays by vibrational cooling on a time scale of several tens of picoseconds. Absorption of free O–H groups around 3530 cm^{-1}, which would be a sign of hydrogen bond breaking,[27] was not observed upon excitation of the O–H/O–D stretching oscillator in our experiments.

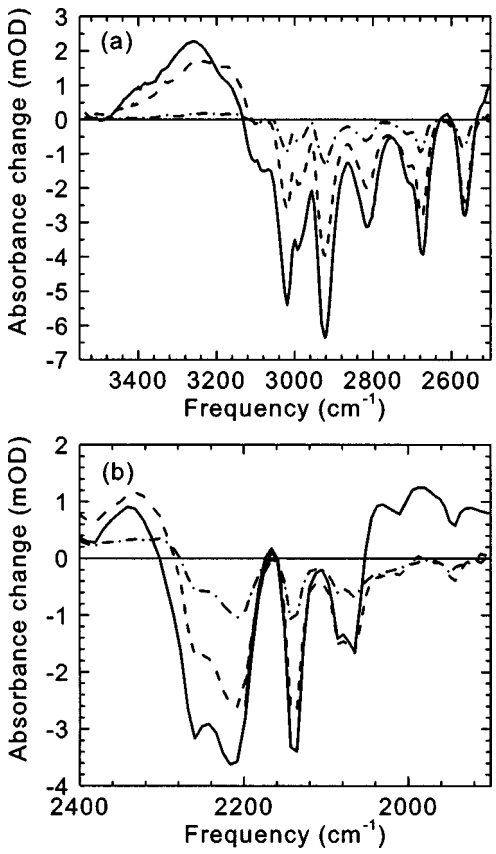

FIG. 6. (a) Transient spectra of the O–H stretching band of cyclic acetic acid dimers I for different pump–probe delay times (solid 0.5 ps, dashed 2.0 ps, and dot-dashed 16 ps) after O–H stretching excitation. (b) Transient spectra of the O–D stretching band of cyclic acetic acid dimers (III) for different pump–probe delay times (solid 0.5 ps, dashed 2.0 ps, and dot-dashed16 ps) after O–D stretching excitation.

Transient spectra at different pump–probe delays [Figs. 6(a) and 6(b)] show a series of spectral dips in the center of the steady-state band which remain unchanged in width and spectral position. This points to a negligible spectral diffusion on a time scale up to 50 ps and a predominant homoge-

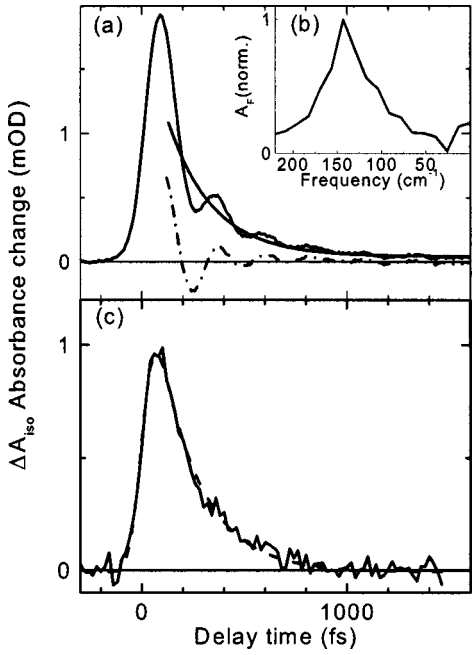

FIG. 7. Pump–probe transients measured for dimers (I) excited at 3000 cm^{-1}. The decay of the excited O–H stretch absorbance ($v=1\rightarrow2$ transition) corrected for rotational relaxation is plotted as a function of delay time for two different probe frequencies. The probe pulses (FWHM≈170 cm^{-1}) are spectrally integrated. (a) Transient at probe frequency centered at 2120 cm^{-1} (solid line), numerical fit (dashed line) and oscillatory signal on top of the noncoherent dynamics (dot-dashed line). (b) Normalized Fourier intensity of the oscillatory signal. (c) Pump–probe transient recorded at a probe frequency centered at 2270 cm^{-1} (solid line) and numerical fit (dashed line).

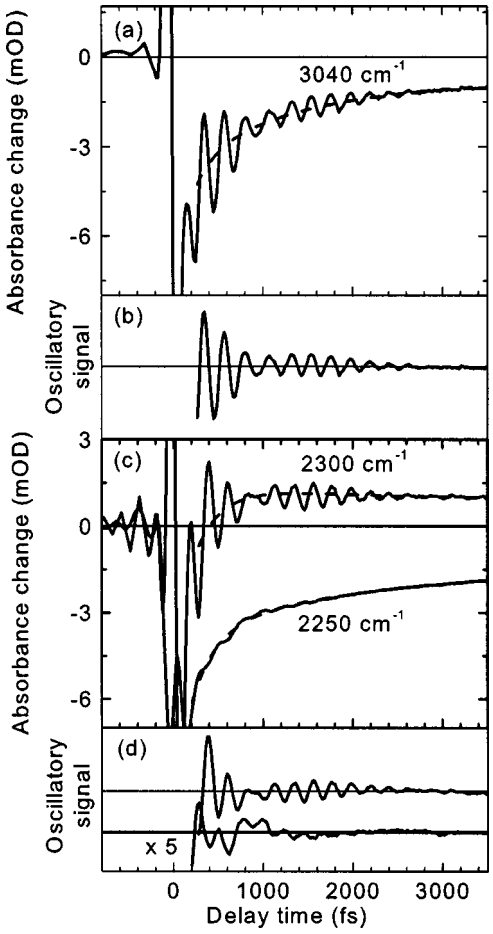

FIG. 8. (a) Absorbance change of the O–H stretching vibration (dimer I) as a function of pump–probe delay (in fs) at a fixed probe frequency at 3040 cm^{-1}. Numerical fits of the incoherent dynamics are shown as smooth dot-dashed curves. The incoherent dynamics can be well reproduced with a fit of three exponentials of 0.2, 1.3, and 15 ps. (b) Residual oscillatory part of the transients at 3040 cm^{-1}. (c) Change of O–D stretching absorbance (dimer III) for probe frequencies at 2300 and 2250 cm^{-1}. Numerical fits of the incoherent dynamics with 0.3, 0.8, and 15 ps are shown as smooth dot-dashed curves. (d) Residual oscillatory part of the transients at 2300 (upper panel) and 2250 cm^{-1} (lower panel). The oscillatory part at 2250 cm^{-1} is multiplied by a factor of 5.

neous broadening of the $\nu_{OH/OD}$ band as has been discussed in more detail in Ref. 30. Such behavior is in sharp contrast to that of systems forming extended hydrogen-bonded networks in the liquid phase like water and/or HOD in D_2O. In such cases, pronounced spectral diffusion has been observed on a multitude of time scales revealing a substantial inhomogeneous broadening of the respective $\nu_{OH/OD}$ bands.[5,8,9]

2. Lifetime of O–H stretching excitations

Measurements with independently tunable pump and probe pulses allowed us to excite the O–H stretching $v=0\rightarrow1$ transition in the center of the O–H stretching band at 3000 cm^{-1} and detect the pure redshifted $v=1\rightarrow2$ transition in a spectral range from 2000 to 2400 cm^{-1} where contributions of the $v=0\rightarrow1$ transition are negligible. Results of such measurements are presented in Fig. 7. The spectrally integrated change of absorbance ΔA_{iso} corrected for rotational diffusion is plotted as a function of delay time for a pump centered at 3000 cm^{-1} and probe pulses centered at 2120 and 2270 cm^{-1} [Figs. 7(a) and 7(c)]. The observed increased absorption is due to the $v=1\rightarrow2$ transition of the O–H stretching vibration (see also Ref. 27) and displays a fast decay after instantaneous rise. The data are well reproduced by a kinetic model [dashed lines in Figs. 7(a) and 7(c)] consisting of an instantaneous rise and an exponential decay with a time constant of 200 fs, convoluted with the cross correlation of pump and probe. On top of the incoherent dynamics a pronounced oscillatory signal with an oscillation period of 240 fs is detected at a probe frequency centered at 2120 cm^{-1}. This corresponds to a frequency of about 145 cm^{-1} as can be seen from the Fourier transformation of the oscillatory signal in Fig. 7(b).

3. Coherent low-frequency motions of cyclic dimers

Time-resolved pump–probe signals with pronounced oscillatory signals are plotted in Fig. 8(a) (solid lines) and Fig. 8(c) (solid lines) for ν_{OH} and ν_{OD} excitation, respectively. The transients were measured at different probe frequencies with ν_{OH} excitation around 2900 cm^{-1} [Fig. 8(a)] and ν_{OD} excitation around 2200 cm^{-1} [Fig. 8(c)]. Perturbed free induction decay and coherent pump–probe coupling contribute to the signals at negative delay times and during the temporal overlap of pump and probe pulses around delay zero. For positive delay times, that is a sequential interaction of pump and probe with the sample, a rate-like increase of absorption is observed which is superimposed by strong oscillations. To isolate the oscillatory signals the incoherent

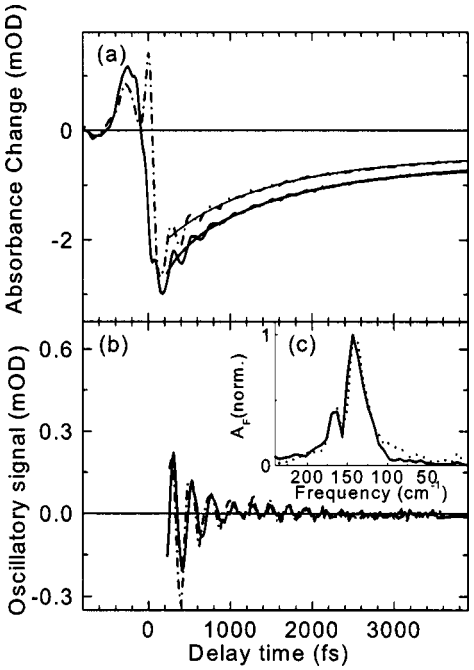

FIG. 9. (a) Time dependent change of the O–H stretching absorbance as a function of time delay between pump at 2950 cm^{-1} and probe at 2880 cm^{-1} of methyl-deuterated acetic acid dimers (I) (solid line) and mixed methyl-deuterated acetic acid dimers (II) (dot-dashed line) dissolved in CCl_4. Transients of dimer (I) and (II) were simulated by a three-exponential fitting function (solid lines) with 0.2, 1.3, and 15 ps and plotted on top of the transients. (b) Difference between total signal and fit for dimer (I) (solid) and dimer II (dot-dashed). (c) Normalized Fourier spectra of the oscillatory transients in b for dimer (I) (solid line) and dimer (II) (dotted line).

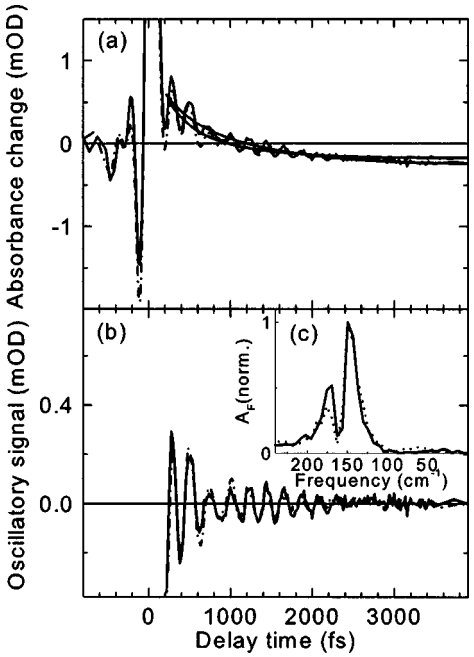

FIG. 10. (a) Time dependent change of the O–D stretching absorbance as a function of time delay between pump at 2100 cm^{-1} and probe at 2020 cm^{-1} of hydroxy-deuterated acetic acid dimers (III) solid line and mixed hydroxy-deuterated acetic acid dimers (IV) dot-dashed line dissolved in CCl_4. Transients of dimer (III) and (IV) were simulated by a three-exponential fitting function (solid lines) with 0.3, 0.8, and 15 ps and plotted on top of the transients. (b) Difference between total signal and fit for dimer (I) (solid) and dimer (II) dot-dashed. (c) Normalized Fourier spectra of the oscillatory transients in (b) for dimer (I) (solid line) and dimer (II) (dotted line).

absorption changes were fitted with three exponentials [Figs. 8(a) and 8(c), dashed lines] for delay times $t_D > 200$ fs and subtracted from the total signal [Figs. 8(b) and 8(d)]. After O–H stretching excitation pronounced coherent signals occur at 3040 cm^{-1} with an oscillation period of 230 fs and a beatnote around 900 fs [Fig. 8(b), upper panel]. This is a clear signature for two different oscillation frequencies contributing to the signal. Similar coherent signals are identified after O–D stretching excitation [Fig. 8(d)]. In Fig. 8(d) (upper panel) the oscillatory component exhibit a period of 220 fs and a beatnote around 900 fs at 2300 cm^{-1}. For probing at 2250 cm^{-1} [Fig. 8(d), lower panel] an additional oscillation frequency with a period of about 1000 fs is found. There is a remarkable similarity of the oscillation frequencies measured after O–H and O–D excitation (cf. Fig. 11). Damping takes place on a time scale of 2–3 ps for both O–H and O–D stretching excitation.

To elucidate the microscopic couplings underlying the coherent signals, experiments with pure cyclic acetic acid dimers are compared to experiments with mixed dimers, which consist of one O–H and one O–D group [Fig. 1, dimers (II), (IV)]. Excitonic coupling does not occur in mixed dimers because of the detuning of the O–H and O–D stretching oscillators.

In Fig. 9, we compare results for methyl-deuterated acetic acid dimers (I) and mixed methyl-deuterated acetic acid dimers (II) with one O–H and one O–D group. The O–H stretching vibration was excited at 2950 cm^{-1} where solely the O–H stretching vibration absorbs and the resulting change of absorbance was detected at 2880 cm^{-1}. For $t_D > 200$ fs, a continuous incoherent increase of absorption is observed superimposed by oscillatory signals up to 2–3 ps. The pump–probe transients of dimer (I) (solid line) and dimer (II) (dot-dashed line) plotted in Fig. 9(a) show very similar temporal behavior. The oscillatory signals obtained after subtracting the rate-like kinetics [solid lines in Fig. 9(a)] are presented in Fig. 9(b) [dimer (I): solid line; mixed dimer (II): dot-dashed line]. Comparison of the coherent signals and their Fourier intensities [Fig. 9(c)] reveal negligible differences. Comparison of the O–D stretching transition and the oscillatory signals of carboxy-deuterated acetic acid dimer (III) with mixed carboxy-deuterated acetic acid dimer with one O–H and one O–D group (IV) leads to similar results (Fig. 10). We studied the dimers (III) and (IV) in a spectral range where the O–H stretching absorption is negligible.

Fourier transformations of the coherent signals for O–H (I) and O–D (III) stretching excitation are plotted in Fig. 11 in comparison to the low-frequency Raman spectrum. The absolute intensities of the Fourier components depend on the spectral position of the probe, whereas the oscillation frequencies remain unchanged throughout the O–H/O–D stretching band. For the purpose of presentation the most prominent oscillatory signals were taken. Two main peaks at 145 and 166 cm^{-1} [Fig. 11(a)] are observed for ν_{OH}, whereas three peaks at 45, 145, and 170 cm^{-1} [Fig. 11(b)] are identified for ν_{OD}. Within the spectral resolution of about

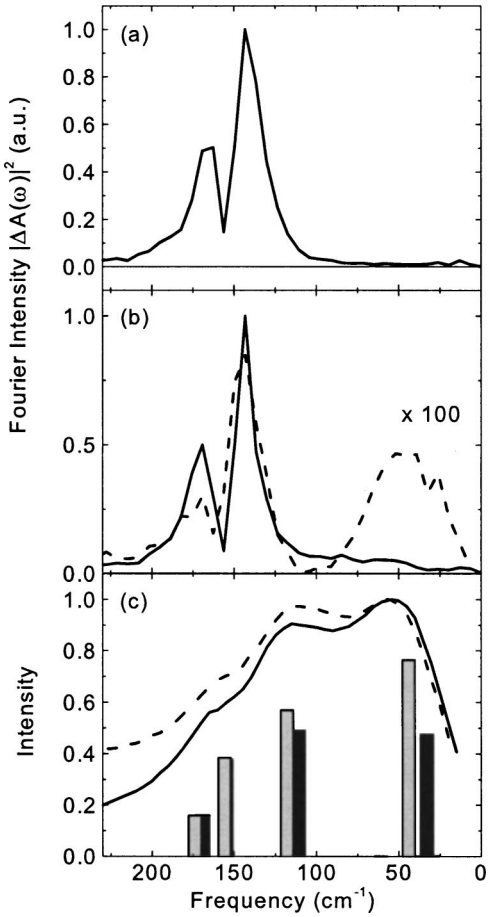

FIG. 11. (a) Fourier intensities of dimer (I) from Fig. 8(b). (b) Fourier intensities of dimer (III) from Fig. 8(d), solid line: at 2300 cm^{-1}, dashed line: at 2250 cm^{-1}. (c) Raman spectrum from Ref. 49 [solid line: $(CH_3COOH)_2$, dashed line: $(CH_3COOD)_2$] together with calculated Raman spectra (Table I): black bars: dimer I, light bars: dimer III.

6 cm^{-1} the spectral positions as well as the intensities of the two peaks at higher frequencies are identical. Towards the high- and low-energy wings of the O–H/O–D spectra the amplitudes increase with some modulations. At the center of the respective stretching bands, i.e., at 3000 cm^{-1} for ν_{OH} and 2250 cm^{-1} for ν_{OD} the time-resolved oscillatory signals display a phase jump by π. A phase difference of $\pi/2$ is observed between the two Fourier components at 145 and 170 cm^{-1}, resulting in the dip between the two peaks at 156 cm^{-1}, where the intensity approaches zero. The two strong components at 145 and 170 cm^{-1} are about two orders of magnitude larger than the component at 50 cm^{-1}. The latter contribution can only be detected near the central part of the O–D absorption band, where the amplitudes of the stronger peaks are diminished because of the phase change by π, so that their contributions are small and do not mask the 50 cm^{-1} component.

V. DISCUSSION

The O–H and O–D stretching dynamics of the hydrogen bonded cyclic dimers directly reflect their different intra- and intermolecular coupling mechanisms. The possible coupling mechanisms such as excitonic coupling, Fermi resonances, or anharmonic coupling to low-frequency modes of the dimers determine the microscopic character of vibrational excitations and provide different channels for energy relaxation which should give rise to different dynamics.

In the following we will discuss the impact of excitonic and Fermi resonance coupling on the dynamics of O–H and O–D stretching excitations. After that we will analyze the coherent dynamics and show how the different coupling mechanisms can be distinguished experimentally by comparing the dynamics of dimers (I)–(IV) (cf. Fig. 1).

A. Relaxation dynamics of O–H and O–D stretching excitations

First, we consider a potential influence of excitonic vibrational coupling on the relaxation dynamics of O–H/O–D stretching excitations. Excitonic coupling of the two O–H stretching oscillators in dimer (I) and the two O–D stretching oscillators in dimer (III) has been invoked in simulations of the steady-state stretching bands and results in a splitting of the $v_{OH/OD}=1$ state (cf. Fig. 3). In the mixed dimers (II) and (IV) with nonresonant O–H and O–D stretching oscillators, excitonic coupling is absent.

In dimer (I), the excited state of the O–H stretching mode ($v_{OH}=1$) decays monoexponentially with a time constant of 200 fs to the hot ground state ($v_{OH}=0'$) in which the O–H stretching oscillator is deexcited and the excess energy of the excitation is transferred to other vibrational modes of the system. Cooling of these accepting vibrational modes by dissipation of the vibrational energy to the surrounding solvent is well simulated by two exponentials with decay constants of 1.3 and 15 ps. The latter time constant is consistent with findings of picosecond studies.[27] The dynamics observed after $v_{OD}=1$ excitation is simulated by a biexponential decay with time constants of 300 and 800 fs, followed by a 15 ps component reflecting vibrational cooling of the hot ground state. In the spectral range of the O–D absorption, the distinction between the depopulation of the $v_{OD}=1$ state and subsequent cooling processes is less clear than for ν_{OH} excitations. In principle, the 800 fs kinetics could represent $v_{OD}=1$ decay processes or be an indication of nonexponential cooling of the hot ground state, similar to the ν_{OH} case.

A comparison of the pure (I,III) and the mixed (II,IV) dimers reveals virtually identical dynamics (Figs. 9 and 10). This observation demonstrates a minor role of excitonic coupling for the time scale and pathways of population relaxation from the $v_{OH}=1$ and $v_{OD}=1$ states.

Next, we discuss the influence of Fermi resonance coupling on the observed dynamics. Fermi resonance coupling in acetic acid dimers may occur between the $v_{OH/OD}=1$ state of the respective stretching vibrations and sufficiently resonant overtone and combination bands. In particular, combination bands of vibrational modes of the carboxyl group such as $\nu_{C\text{-}O}$, $\nu_{C=O}$, or $\delta_{OH/OD}$ have been suggested to play an important role for Fermi coupling.[20,24,25] Fermi coupling leads to a mixing of the states involved and accordingly, to frequency shifts. For the case of weak coupling, the states essentially keep their original character. For strong coupling, however, the mixed states may contain similar contributions

from the original uncoupled basis states. These two cases may be distinguished experimentally. For weak coupling, the dynamics should depend on the excitation wavelength, because excited states of different character are likely to exhibit different dynamics. For strong coupling, however, the character of the states is very similar and thus, similar dynamics are expected. Because we do not observe any wavelength dependence in our dynamics, we conclude that Fermi coupling is strong in acetic acid dimers. This conclusion is supported by experiments on O–H bending modes of acetic acid dimers[52] and calculations of acetic acid dimers and related compounds.[20,24,25]

The total strength of Fermi resonance interaction of the O–H stretching mode is reported to be more than two times larger than that of the O–D stretching vibration.[20] Fermi coupling is therefore expected to lead to isotope effects of the dynamics. The observation that the O–H modes exhibit a faster decay of the $v_{\mathrm{OH}}=1$ state than the O–D mode supports a stronger Fermi resonance interaction of ν_{OH} compared to ν_{OD}. In both cases, further experiments are required to clarify the pathways of population relaxation. First two-color pump–probe experiments have revealed a strong anharmonic coupling of the O–H stretching mode to the infrared active O–H bending mode and the C–O stretching mode in the cyclic dimer.[52] Such measurements demonstrate a negligible relaxation induced excess population of the $v=1$ state of the infrared-active bending mode and suggest that a multitude of modes is involved in the relaxation of O–H stretching excitations.

It should be noted that we do not observe hydrogen bond breaking after O–H stretching excitation as discussed in Ref. 27. The higher time resolution and the small amount of molecules excited in our measurements suppress heating effects as well as sequential and two-photon excitation and we conclude that hydrogen bond breaking is negligible upon single photon excitation.

B. Coherent wavepacket motions along low-frequency modes

The incoherent dynamics of the O–H/O–D stretching excitations is superimposed by oscillatory signals denoting nuclear wavepacket motions (Figs. 7–10). The femtosecond broadband pump pulse creates a coherent superposition of vibrational quantum states oscillating with their difference frequencies. The nature of the created wavepackets depends on the character of the states involved in the superposition. In the following, we consider three mechanisms potentially underlying the observed behavior, i.e., (i) excitonic or Davydov coupling, (ii) Fermi resonances, and (iii) anharmonic coupling to low-frequency modes.

(i) A quantum beat due to a coherent superposition of excitonically split $v_{\mathrm{OH/OD}}$ states in a single dimer can be ruled out by dipole selection rules.[19] The excitonic coupling of the two identical O–H/O–D stretching oscillators leads to a splitting of the $v_{\mathrm{OH/OD}}=1$ states and to $v^{+}_{i,Qu}$ and $v^{-}_{i,Qu}$ levels (cf. Fig. 3) with different dipole selection rules. Transitions to the $v^{-}_{i,Qu}$ levels of a low-frequency mode are only allowed from the $v_{Qu}=0$ level of the $Q_{i,u}$ mode in the $v_{\mathrm{OH/OD}}=0$ state and to the $v^{+}_{i,Qu}$ levels from the $v_{Qu}=1$ level of the $Q_{i,u}$ mode in the $v_{\mathrm{OH/OD}}=0$ state. Due to the fact that a specific molecule that is in thermal equilibrium with its surrounding does not exist in the $v_{Qu}=0$ and $v_{Qu}=1$ levels simultaneously, a coherent superposition of excitonically split levels, i.e., a quantum beat, cannot occur. The spectrally resolved pump–probe signal $\Delta A(\omega,t_D)\propto \mathrm{Im}[P^{(3)}(\omega,t_D)/E_{pr}(\omega)]$ is proportional to the imaginary part of the third order nonlinear polarization $P^{(3)}(\omega,t_D)$ [$E_{\mathrm{pr}}(\omega)$: electric field of the probe pulse]. The pump–probe signal depends linearly on $P^{(3)}(\omega,t_D)$ and molecules initially populating different levels of the low-frequency modes in the $v_{\mathrm{OH/OD}}=0$ state contribute additively to the overall third-order polarization. Thus, interferences between emitted third order nonlinear polarizations of different molecules are absent, i.e., there are no contributions oscillating with a frequency determined by the excitonic splitting. This conclusion is supported independently by our experiments with the mixed dimers (II) and (IV) in which excitonic coupling does not occur. Such mixed dimers exhibit the same oscillatory signals as the dimers (I) and (III).

(ii) A coherent superposition of states split by Fermi resonances can only be detected as long as the coherence between the states exists. The dephasing time T_2 of the ν_{OH} $0\rightarrow1$ transition was determined by femtosecond three-pulse photon echo studies to be $\approx$200 fs.[30] Additionally, an upper limit for the dephasing time T_2 is given by $T_2\leqslant 2T_1$ (T_1: population relaxation time), that is several hundred femtoseconds for the $v_{\mathrm{OH/OD}}=1$ state. Thus, oscillatory signals observed at picosecond delay times cannot result from excited $v_{\mathrm{OH/OD}}$ states, but have to be due to wave packet motion in the ground ($v_{\mathrm{OH/OD}}=0$) vibrational state.

Theoretical as well as experimental investigations[20,24,25] have suggested that several Fermi resonances with different splittings of the coupled states occur within the broad O–H/O–D stretching bands. If such states underlie the oscillatory signals, one expects a change of oscillation frequency with the spectral position of the probe pulse. The fact that we do not observe any wavelength and isotope dependence of the oscillation frequencies throughout the stretching bands also demonstrates a minor role of Fermi resonances.

(iii) We now consider the anharmonic coupling to low-frequency states. Excitation of the $v_{\mathrm{OH/OD}}=1$ level by the pump pulse creates a nonstationary coherent superposition of anharmonically coupled low-frequency states within the pump bandwidth, giving rise to the oscillations in the excited vibrational state (cf. Fig. 3). Equally likely, a coherent superposition of low-frequency states in the $v_{\mathrm{OH/OD}}=0$ state is generated through an impulsive Raman process within the pump bandwidth. We observe identical oscillation frequencies in the pure excited state ($v_{\mathrm{OH/OD}}=1$) transients (dimer I, Fig. 7), which strongly suggests that the character of wave packet motion is identical in the $v_{\mathrm{OH/OD}}=0$ and 1 states. In agreement with this picture, the oscillation frequencies are not altered upon changing the pump and probe frequencies in the range of the O–H/O–D absorption band. The Raman process generating vibrational coherence in the $v_{\mathrm{OH/OD}}=0$ state is resonantly enhanced by the O–H/O–D stretching absorption. This is evident from a phase jump of π in the oscillatory signal at the center of the respective absorption

band, i.e., around 3000 cm^{-1} for the O–H case and around 2250 cm^{-1} for the O–D case.

The character of the wavepacket motion can be deduced from an analysis of the low-frequency Raman spectrum. The agreement between our DFT calculations discussed in Sec. III and the experimental steady-state spectrum is very good, with respect to both vibrational frequencies and intensities [Fig. 11(c)]. We assign the band observed at 50 cm^{-1} to the τ_{bg} methyl torsion mode. The band at 118 cm^{-1} is assigned to the γ_{bg} dimer oop wagging mode. The broad band around 170 cm^{-1}, which was fitted to two bands at 165 and 185 cm^{-1},[50] is attributed to the δ_{ag} dimer ip bending and ν_{ag} dimer stretching modes. Experimental[49] and theoretical depolarization ratios are in accordance for all four low-frequency modes.

The Fourier components of 145 and 170 cm^{-1} of the coherent signals are identical for $(CD_3COOH)_2$ [Fig. 11(a)] and $(CH_3COOD)_2$ [Fig. 11(b)] within the experimental accuracy and bandwidth of the peaks. They are attributed to the δ_{ag} and ν_{ag} modes. The additional component at 50 cm^{-1} which is observed for ν_{OD} excitation and assigned to the τ_{bg} mode, probably exists for ν_{OH} excitation as well, but it remains hidden under the strong modulations of the higher-frequency components. The Fourier component at 145 cm^{-1} is always found to be somewhat stronger than the peak at 170 cm^{-1}. It is important to note that the sign of the phase changes by about $\pi/2$ between the two peaks. The peak at 50 cm^{-1} is always very small compared to the other two. A peak around 118 cm^{-1} is not observed. This pattern is in agreement with the calculated cubic anharmonic coupling constants Φ between the high-frequency $\nu_{OH/OD}$ and the low-frequency modes (Fig. 4, Table I). Opposite signs of the coupling constants of the 145 and 170 cm^{-1} component indicate different phases. In contrast to the steady-state Raman spectrum, the pump–probe data allow for a clear spectroscopic separation of the δ_{ag} and ν_{ag} bands demonstrating the potential of nonlinear spectroscopy for analyzing low-frequency vibrational spectra. It should be noted that the strength of the Fourier components depends not only on the anharmonic couplings Φ. The spectral width of the electric field envelope of the pump pulses defines the frequency range in which low-frequency modes are excited. In addition, the dephasing times of the different modes influence the strength of the Fourier components. In the present case, the three low-frequency motions show similar picosecond dephasing times.

In contrast to the two ip bending and stretching modes of a_g symmetry, anharmonic coupling to the b_g symmetric oop wagging mode is calculated to be zero in all cases, in agreement with our experiments. This is plausible, because the ip modes modulate the hydrogen bond distance strongly, whereas the oop mode mostly entails small angle distortions. Carboxy deuteration does not lead to isotopic shifts of the methyl torsion and dimer stretching modes, whereas the dimer ip bending mode shifts by -3 cm^{-1}. This shift is well below the experimental detection limit.

VI. CONCLUSIONS

Femtosecond two-color mid-infrared pump–probe spectroscopy combined with *ab initio* calculations based on density functional theory demonstrates the important role of anharmonic coupling to low-frequency modes for the dynamics of the hydrogen bonded O–H/O–D stretching vibrations of cyclic acetic acid dimers. Anharmonic coupling to low-frequency modes is shown to be responsible for the pronounced underdamped coherent oscillations observed in the nonlinear O–H/O–D stretching absorption. In contrast, excitonic coupling of two identical O–H or O–D stretching oscillators and Fermi resonances do not contribute to the wave packet motion. Based on the comparison to *ab initio* calculated low-frequency Raman modes and their anharmonic couplings to the high-frequency O–H/O–D stretching vibrations we assign the modes contributing to coherent motions to the ip dimer stretching (170 cm^{-1}) and bending (145 cm^{-1}) and the methyl torsion mode (50 cm^{-1}). The ip interdimer modes couple strongly, in contrast to the methyl torsion mode. The oop dimer mode calculated at 118 cm^{-1} is uncoupled.

Population relaxation of the $v_{OH/OD}=1$ states of the stretching oscillators occurs on a subpicosecond time scale. The relaxation times of the excitonically coupled O–H or O–D oscillators in pure dimers and of single O–H or O–D oscillators in mixed dimers are very similar, pointing to a minor influence of excitonic coupling on the relaxation behavior. Fermi resonance coupling in acetic acid dimers is generally strong. Fermi coupling is stronger for ν_{OH} than for ν_{OD} as is manifested by a faster decay of the $v_{OH}=1$ state than of the $v_{OD}=1$ state.

Anharmonic coupling strengths of combination bands resulting from stretching and bending vibrations of the carboxy group are on the same order as anharmonic couplings to low-frequency modes.[48] Thus, both coupling mechanisms, Fermi resonances, and anharmonic coupling to low-frequency modes, are expected to provide efficient energy relaxation pathways.

Carboxylic acid dimers represent important model systems displaying key features of hydrogen bonded systems in nature. Ultrafast nonlinear mid-infrared spectroscopy in connection with anharmonic *ab initio* calculations allows for a detailed understanding of the microscopic coupling mechanisms and interactions of hydrogen bonds determining the structure and functionality of numerous biomolecules.

ACKNOWLEDGMENTS

This research was supported by the Deutsche Forschungsgemeinschaft (Sonderforschungsbereich 450, Teilprojekt B2). S.M. is grateful for the support of the National Institutes of Health Grant No. 1 RO1 GM59230-10A2.

[1] D. Hadži and S. Bratos, in *The Hydrogen Bond*, edited by P. Schuster, G. Zundel, and S. Sandorfy (Elsevier, Amsterdam, 1976), Chap. 12, p. 565.
[2] For a review: *Ultrafast Hydrogen Bonding Dynamics and Proton Transfer Processes in the Condensed Phase*, T. Elsaesser and H. J. Bakker (Kluwer, Dordrecht, 2002).
[3] E. T. J. Nibbering and T. Elsaesser, Chem. Rev. **104**, 1887 (2004).
[4] J. Stenger, D. Madsen, P. Hamm, E. T. J. Nibbering, and T. Elsaesser, Phys. Rev. Lett. **87**, 027401 (2001).

[5] J. Stenger, D. Madsen, P. Hamm, E. T. J. Nibbering, and T. Elsaesser, J. Phys. Chem. A **106**, 2341 (2002).
[6] J. C. Deàk, S. T. Rhea, L. K. Iwaki, and D. D. Dlott, J. Phys. Chem. A **104**, 4866 (2000).
[7] S. Yeremenko, M. S. Pshenichnikov, and D. A. Wiersma, Chem. Phys. Lett. **369**, 107 (2003).
[8] H. J. Bakker, H.-K. Nienhuys, G. Gallot, N. Lascoux, G. Gale, J. C. Leicknam, and S. Bratos, J. Chem. Phys. **116**, 2592 (2002).
[9] G. M. Gale, G. Gallot, F. Hache, N. Lascoux, S. Bratos, and J.-C. Leicknam, Phys. Rev. Lett. **82**, 1068 (1999).
[10] S. Woutersen and H. Bakker, Phys. Rev. Lett. **83**, 2077 (1999).
[11] C. J. Fecko, J. D. Eaves, J. J. Loparo, A. Tokmakoff, and P. L. Geissler, Science **301**, 1698 (2003).
[12] R. Laenen, C. Rauscher, and A. Laubereau, Phys. Rev. Lett. **80**, 2622 (1998).
[13] C. P. Lawrence and J. L. Skinner, J. Chem. Phys. **117**, 5827 (2002).
[14] A. Piryatinski, C. P. Lawrence, and J. L. Skinner, J. Chem. Phys. **118**, 9664 (2003).
[15] R. Rey, K. B. Møller, and J. T. Hynes, J. Phys. Chem. A **106**, 11993 (2002).
[16] J. Stenger, D. Madsen, J. Dreyer, E. T. J. Nibbering, P. Hamm, and T. Elsaesser, J. Phys. Chem. A **105**, 2929 (2001).
[17] D. Madsen, J. Stenger, J. Dreyer, E. T. J. Nibbering, P. Hamm, and T. Elsaesser, Chem. Phys. Lett. **341**, 56 (2001).
[18] D. Madsen, J. Stenger, J. Dreyer, P. Hamm, E. T. J. Nibbering, and T. Elsaesser, Bull. Chem. Soc. Jpn. **75**, 909 (2002).
[19] Y. Marechal and A. Witkowski, J. Chem. Phys. **48**, 3697 (1968).
[20] Y. Maréchal, J. Chem. Phys. **87**, 6344 (1987).
[21] Y. Fujii, H. Yamada, and M. Mitzuta, J. Phys. Chem. **92**, 6768 (1988).
[22] D. Chamma and O. Henri-Rousseau, Chem. Phys. **248**, 53 (1999).
[23] D. Chamma and O. Henri-Rousseau, Chem. Phys. **248**, 71 (1999).
[24] G. M. Florio, T. S. Zwier, E. M. Myshakin, K. D. Jordan, and E. L. Sibert III, J. Chem. Phys. **118**, 1735 (2003).
[25] C. Emmeluth, M. A. Suhm, and D. Luckhaus, J. Chem. Phys. **118**, 2242 (2003).
[26] M. Lim and R. M. Hochstrasser, J. Chem. Phys. **115**, 7629 (2001).
[27] G. Seifert, T. Patzlaff, and H. Graener, Chem. Phys. Lett. **333**, 248 (2001).
[28] K. Heyne, N. Huse, E. T. J. Nibbering, and T. Elsaesser, J. Phys.: Condens. Matter **15**, S129 (2003).
[29] K. Heyne, N. Huse, E. T. J. Nibbering, and T. Elsaesser, Chem. Phys. Lett. **369**, 591 (2003).
[30] N. Huse, K. Heyne, J. Dreyer, E. T. J. Nibbering, and T. Elsaesser, Phys. Rev. Lett. **91**, 197401 (2003).
[31] S. Bratos and D. Hadži, J. Chem. Phys. **27**, 991 (1957).
[32] N. Sheppard, in *Hydrogen Bonding*, edited by D. Hadži (Pergamon, London, 1959), p. 85.
[33] M. J. Wojcik, A. Y. Hirakwara, and M. Tsuboi, Int. J. Quantum Chem., Quantum Biol. Symp. **13**, 133 (1986).
[34] D. Chamma and O. Henri-Rousseau, Chem. Phys. **248**, 91 (1999).
[35] R. Rey and J. T. Hynes, J. Chem. Phys. **104**, 2356 (1994).
[36] C. Lee, R. G. Yang, and W. Parr, Phys. Rev. B **37**, 785 (1988).
[37] B. Miehlich, A. Savin, H. Stoll, and H. Preuss, Chem. Phys. Lett. **157**, 200 (1989).
[38] A. D. Becke, J. Chem. Phys. **98**, 5648 (1993).
[39] R. H. Hertwig and W. Koch, Chem. Phys. Lett. **268**, 345 (1997).
[40] A. D. McLean and G. S. Chandler, J. Chem. Phys. **72**, 5639 (1980).
[41] R. Krishnan, J. S. Binkley, and R. Seeger, J. Chem. Phys. **72**, 650 (1980).
[42] T. Clark, J. Chandrasekhar, G. W. Spitznagel, and P. V. R. Schleyer, J. Comput. Chem. **4**, 294 (1983).
[43] M. J. Frisch, G. W. Trucks, H. B. Schlegel *et al.*, GAUSSIAN 98 Revision A.9, Gaussian, Inc., Pittsburgh, PA, 1998.
[44] W. Schneider and W. Thiel, Chem. Phys. Lett. **157**, 367 (1989).
[45] S. Dressler and W. Thiel, Chem. Phys. Lett. **273**, 71 (1997).
[46] T. Nakabayashi, H. Sato, F. Hirata, and N. Nishi, J. Phys. Chem. A **105**, 245 (2001).
[47] J. Chocholoušová, J. Vacek, and P. Hobza, J. Phys. Chem. A **107**, 3086 (2003).
[48] J. Dreyer (unpublished).
[49] O. F. Nielsen and P.-A. Lund, J. Chem. Phys. **78**, 652 (1983).
[50] T. Nakabayashi, K. Kosugi, and N. Nishi, J. Phys. Chem. A **103**, 8595 (1999).
[51] R. A. Kaindl, M. Wurm, K. Reimann, P. Hamm, A. M. Weiner, and M. Woerner, J. Opt. Soc. Am. B **17**, 2086 (2000).
[52] K. Heyne, N. Huse, E. T. J. Nibbering, and T. Elsaesser, Chem. Phys. Lett. **382**, 19 (2003).